PCCP

Accepted Manuscript

How can $[\mathrm{Mo^{IV}(CN)_6}]^{2-}$, an apparently octahedral $(\mathrm{d})^2$ complex, be diamagnetic? Insights from quantum chemical calculations and magnetic susceptibility measurements.[†]

Mariusz Radoń[*1], Paweł Rejmak[2], Magdalena Fitta[3],

Maria Bałanda[3], and Janusz Szklarzewicz[*1]

[1]Department of Chemistry, Jagiellonian University in Kraków, Kraków, Poland

[2]Institute of Physics, Polish Academy of Sciences, Warsaw, Poland

and Donostia International Physics Center, San Sebastian, Spain

[3]Institute of Nuclear Physics, Polish Academy of Sciences, Kraków, Poland

_____

[*] Electronic addresses: `mradon@chemia.uj.edu.pl`; `szklarze@chemia.uj.edu.pl`; Corresponding authors.

[†] Electronic Supplementary Information (ESI) available. Optimized Cartesian coordinates, plots of molecular orbitals, additional computational results, pseudopotentials and structures optimized in periodic DFT calculations, magnetic susceptibility data, and derivation of the theoretical model to explain temperature dependence of the magnetic susceptibility for a system with close lying singlet and triplet states.

Abstract

Quantum chemical calculations are employed to elucidate the origin of a puzzling diamagnetism for hexacyanomolybdate(IV) anion, $[\text{Mo(CN)}_6]^{2-}$, that was previously reported by Szklarzewicz *et al.* [*Inorg. Chem.*, **2007**, *46*, 9531–9533]. The diamagnetism is surprising because for the octahedral $(\text{d})^2$ complex one would rather expect a (paramagnetic) triplet ground state, clearly favored over a (diamagnetic) singlet state by an exchange interaction between two d electrons in the t_{2g} orbitals. Nevertheless, the present calculations reveal that the minimum energy structure of isolated $[\text{Mo(CN)}_6]^{2-}$ is not an octahedron, but a trigonal prism; the latter geometry allows to maximize a σ-donation from the cyanides to the electron-deficient Mo(IV) center. Unlike for the octahedron, for the trigonal prism structure the singlet and triplet spin states are close in energy to within a few kcal/mol. Although the actual relative energy of the two spin states turns out to be method-dependent, the complete active space calculations (CASPT2; with appropriate choice of the IPEA shift parameter) can reproduce the singlet ground state, in agreement with the experimentally observed diamagnetism. Moreover, magnetic measurements reveal a slight increase of the magnetic susceptibility with the increase of temperature from 100 to 300 K, suggesting an admixture of a thermally induced paramagnetism (possibly due to Boltzmann population of the low-energy triplet state) on top of the dominant diamagnetism. Our prediction that the geometry of $[\text{Mo(CN)}_6]^{2-}$ should significantly deviate from the ideal octahedron, not only in gas phase, but also in periodic DFT model of the crystalline phase, as well as the experimentally confirmed diamagnetic properties, do not agree with the previously reported ideal octahedral structure. We suggest that this crystal structure might have been determined incorrectly (e.g., due to overlooked merohedral twinning or superstructure properties) and it should be re-investigated.

1   Introduction

A number of transition metal complexes have two (or more) spin states so close in energy, that to predict which of them is actually the ground state, one has to calculate their relative energy with a high accuracy. Such calculations are, in general, challenging for quantum chemistry, requiring either carefully calibrated density functional theory (DFT) methods or high-level correlated wave function methods, in order to reproduce a delicate balance between the bonding and the exchange-correlation effects, which determines the spin-state energetics[1–4]. But for some complexes the situation is much simpler because the multiplicity of the ground state can be easily established based on the Hund's rule of maximum multiplicity[5]. For instance, an octahedral complex with the $(d)^2$ central ion should have a high-spin (triplet, $S = 1$) ground state, clearly favored over a low-spin (singlet, $S = 0$) state by an exchange interaction of two electrons distributed in the t_{2g} orbitals. For this reason, any octahedral $(d)^2$ complex is expected to be paramagnetic.

Given the above, it was a great surprise to see in the previous study[6] that tetramethylammonium hexacyanomolybdate(IV), $(Me_4N)_2[Mo^{IV}(CN)_6] \cdot H_2O$ (**1**), is *diamagnetic* although its crystal structure revealed the $[Mo^{IV}(CN)_6]^{2-}$ anion in the perfectly octahedral geometry[6]. For the octahedral complex of Mo(IV) one would rather expect the triplet ground state ($^3T_{1g}$; arising from two d electrons in the t_{2g} manifold) and thus, obviously, a paramagnetic character. The purpose of this paper is to elucidate this paradoxical result by means of quantum chemical calculations and interpretation of magnetic susceptibility measurements.

We notice that cyanide complexes of transition metals are considered as prospective building blocks for new magnetic materials[7,8]. It is thus important to thoroughly understand their electronic properties and relation thereof to the molecular structure, particularly for cases as puzzling as the present one. Therefore, in this paper we shall consider various effects that might be responsible for the unexpected dia-

magnetism of $[Mo(CN)_6]^{2-}$, including a possibility of magnetic coupling between the neighboring anions in the crystal structure of **1**, effects of the spin-orbit coupling, and distortions from the ideal octahedral geometry. In fact, our calculations will suggest that $[Mo(CN)_6]^{2-}$ tends to adopt a non-octahedral, trigonal-prismatic structure, which may be presumably the primary factor leading to stabilization of the low-spin state. The relative spin-state energetics of $[Mo(CN)_6]^{2-}$ will be studied with a number of DFT and wave function theory methods. Finally, the magnetic properties will be theoretically simulated and compared with the experimental magnetic susceptibility data for a wide range of temperatures.

2 Computational and experimental details

2.1 Molecular DFT calculations

DFT calculations for an isolated $[Mo(CN)_6]^{2-}$ were carried out with `Turbomole`[9] and `Gaussian 09`[10] packages. The structures were optimized and harmonic frequencies were computed (to verify the character of stationary points and to yield zero-point energies and thermal vibrational corrections to the Gibbs free energy) at the DFT:BP86/def2-TZVP[11] level in `Turbomole`. Subsequently, single-point calculations were carried out with a larger basis set (def2-QZVPP for Mo, def2-TZVPP for C and N)[12] and employing a number of functionals: BP86[13], PBE[14], B3LYP[15], TPSS[16], TPSSh[17], B2PLYP[18] (in `Turbomole`), B3LYP*[19], OLYP[20], M06, M06L[21] (in `Gaussian 09`).

The triplet state was treated within the spin-unrestricted formalism, whereas for the singlet state we considered either a spin-restricted (closed-shell) or a spin-unrestricted (open-shell) description. The final energy of the open-shell singlet solution was corrected for spin contamination using the approximate spin-projection method of Yamagushi *et al.*[22]. The spin-restricted singlet solution has been found to

be unstable (triplet instability) and giving higher energy than the spin-unrestricted solution (except for B2PLYP, where the spin-restricted solution was found 1.3 kcal/mol lower in energy than the spin-unrestricted solution after the projection).

The calculated structural parameters are summarized in Table S2, ESI†. The optimum geometry for the closed-shell singlet solution is the ideal trigonal prism (D_{3h} symmetry). For the triplet as well as for the open-shell singlet solution, the optimum geometry is a slightly distorted trigonal prism (C_{2v} and C_s symmetry, respectively). Concerning the octahedral geometry, we considered in addition to the ideal O_h structure (from the crystal structure of **1**, ref. 6) also the structures partially optimized at the DFT:BP86 level under the D_{2h} symmetry constraints (to keep the NC–Mo–CN angles as in the octahedron, i.e., 90° or 180°, but allow to partly break the ideal O_h symmetry due to uneven occupation of the t_{2g} level; the actual symmetry turned out to be slightly higher than enforced, namely D_{4h}). However, these octahedral structures turned out to be saddle points whose imaginary frequencies correspond to deformation modes of the octahedron; see Table S2, ESI†. The relative singlet–triplet energy obtained from both the ideal octahedral structure from ref. 6 and the mentioned, partially optimized octahedral structures are similar to within 1–2 kcal/mol (see Table S3, ESI†).

To estimate the magnetic coupling between the nearest neighbor $[Mo(CN)_6]^{2-}$ octahedra in the triplet state, we used a two-center model $[Mo(CN)_6]^{2-}\cdots H_2O\cdots[Mo(CN)_6]^{2-}$ (Figure S1, ESI†) whose coordinates were taken from the crystal structure of **1**. Because the positions of the hydrogen atoms in this crystal structure have not been refined in ref. 6 (the water H atoms were placed, with fractional occupations at eight symmetry-equivalent positions imposed by the space group), we adjusted them by setting the H−O−H angle to 104.5° and orienting the water molecule so that it forms two H-bonds with CN groups of the neighboring octahedra (cf Figure S1, ESI†). We considered two spin states for

the dimer model, obtained by either either ferro- ($S_{tot} = 2$) or antiferromagnetic ($S_{tot} = 0$) coupling of the two triplet spins $S_1 = S_2 = 1$ of the Mo atoms, and compared the total energy for these two spin couplings. The calculations were performed at the DFT/def2-SV(P) level with two exchange-correlation functionals: B3LYP and BP86 and, for comparison, also at the B3LYP/def2-TZVPP(Mo, H)/ma-TZVPP(C,N,O) level, where the basis set is augmented with diffuse functions[23] on C, N, and O atoms.

The Karlsruhe (def2-) basis sets used in the DFT calculations include scalar-relativistic effects for Mo via the effective core potential[11]. However, test calculations were also carried out with ADF[24] employing the zero-order regular approximation (ZORA)[25] to describe both scalar and spin-orbit effects; the BP86 functional and the appropriate TZ2P basis from the ADF library were used in these DFT-ZORA calculations.

The scan of potential energy surface along the Bailar twist coordinate, shown in Figure 2, has been generated at the BP86/def2-TZVP level (in `Turbomole`) by performing a series of constrained optimizations. The applied geometry constraints are defined in Figure S8, ESI†. The initial structures for selected points $0° \leq \theta \leq 60°$ were generated from the experimental octahedral geometry using the appropriately defined Z-matrix (Table S19, ESI†).

The intrinsic reaction coordinate (IRC) paths were computed with `Gaussian` at the BP86/def2-TZVP level, employing local quadratic approximation (LQA) with analytic Hessian computed at every point. The maximum number of points was considerably increased (to 100) to ensure completing the IRC computation. The IRC started from the octahedral geometry of each spin state (first optimized under D_{2h} symmetry constraints) following the normal coordinate eigenvector with the largest imaginary frequency. After `Gaussian` completed the computation of the path, harmonic frequencies were calculated for the last point, still revealing the presence

6

of (one or two) imaginary frequencies. Such a behavior suggests the closeness of another saddle point on the reaction path without an intervening minimum, which is indicative of a bifurcation behavior[26]. Indeed, we were able to locate a saddle point very close in energy (< 0.1 kcal/mol) to the last point of the IRC path. Therefore, the reaction path was continued by starting a new IRC computation from last point of the previous IRC path; we repeated this procedure, if necessary, until all frequencies were real at the final point of the last IRC path. In this way we generated in total two (singlet restricted) or three (singlet unrestricted, triplet) consecutive IRC paths, labeled throughout as IRC-1, IRC-2, and IRC-3. After reaching the last point of the last IRC, the structure was normally optimized to the energy minimum. Schemes and animated movies of the IRC paths are given in the ESI†.

Born-Oppenheimer molecular dynamics (MD) simulations were performed in `Turbomole 6.5` at the BP86/def2-TZVP level, with the integration time step of 80 a.u. (~ 1.9 fs), starting from the experimental octahedral geometry. The simulations were performed within canonical ensemble for $T = 300$ K employing the Noosé–Hoover thermostat with a relaxation time of 200 a.u. Animated movies of the resulting MD trajectories are provided in the ESI†.

2.2 Periodic DFT calculations

Periodic DFT calculations were carried out with `Siesta`[27]. The cubic unit cell was based on the crystal structure of **1** from ref. 6: $a = b = c = 12.59$ Å, $\alpha = \beta = \gamma = 90°$; this unit cell contains four $[\text{Mo(CN)}_6]^{2-}$ anions, eight $(\text{CH}_3)_4\text{N}^+$ cations, and four water molecules. We note that although it is possible to choose a smaller (rhombohedral) primitive cell with just one $[\text{Mo(CN)}_6]^{2-}$, we decided to use the larger one in order to not impose an equivalency of all the $[\text{Mo(CN)}_6]^{2-}$ anions. However, test calculations were performed for the rhombohedral cell, and revealed

a qualitatively similar distortion of the anion from the octahedral geometry as found for the larger cell.

The initial atomic coordinates inside the unit cell were based on the previously reported crystal structure[6] (Cambridge code: HITPOQ). However, in order to facilitate the calculation, a single orientation was arbitrarily chosen for the disordered $(CH_3)_4N^+$ cations and water molecules. We optimized the atomic coordinates in the fixed unit cell using the conjugate-gradient optimizer until the maximum atomic force was not larger than 0.04 eV/Å. Separate optimization was carried out assuming the global closed-shell singlet state (i.e., all $[Mo(CN)_6]^{2-}$ units in the singlet state) and the global $S = 4$ state (i.e., all $[Mo(CN)_6]^{2-}$ units in the triplet state).

Brillouin zone sampling was restricted to the Γ point. PBE exchange-correlation functional[14] with the Grimme's dispersion correction (DFT-D2)[28] was applied. We used the numeric atomic orbitals DZP quality basis set with orbital confinement controlled by energy shift value set to 0.0025 a.u. Norm conserving Troullier-Martins pseudopotential[29], as generated with the `atom` utility, were employed. For Mo, 4p semicore orbitals were included in valence; relativistic and pseudocore corrections were applied to the pseudopotential. The pseudopotentials are provided in the ESI†. The density of grid used for the DFT calculations were controlled by a mesh cutoff value of 400 Ry.

2.3 Complete active space calculations

CASSCF/CASPT2 calculations were carried out with `Molcas 7.8`[30] for the octahedral structure of $[Mo(CN)_6]^{2-}$ taken from the literature crystal structure of **1** as well as for the DFT:BP86-optimized geometries of the singlet and triplet states, revealing the trigonal prismatic structure. We found that at the CASPT2 level the lowest singlet state has lower an energy when calculated for the more symmetric structure corresponding to the spin-restricted singlet (D_{3h}) than for the structure of

the spin-unrestricted singlet (C_s). Therefore, the CASPT2 results reported here for the singlet state refer to the D_{3h} structure.

The active space for the octahedral structure was constructed using the standard approach for transition metal complexes, i.e., by making active five 4d orbitals of Mo and two combinations of the CN lone pairs (of e_g symmetry) which participate in the σ-type bonding with Mo; i.e., 6 active electrons distributed in 7 active orbitals. However, this small active space is not adequate for the trigonal prismatic structure due to appearance of additional metal–ligand interactions, which can be taken into account by making active two more combinations of the cyanide lone pairs (of e' symmetry in D_{3h}). Since the added cyanide orbitals are strongly mixed with the Mo 4p orbitals, the latter have to be added as well. Finally, double-shell d orbitals on Mo were also added for the partially filled d orbitals of the a'_1 and e' symmetry, yielding in total the active space of 16 electrons in 15 active orbitals. The contour plots of the active orbitals can be found in Figure S7, ESI†.

To take into account all the singlet and triplet states emerging from the $(t_{2g})^2$ configuration for the octahedron (i.e., $^1T_{2g} + ^1E_g + ^1A_{1g} + ^3T_{1g}$) and the corresponding $(a'_1, e')^2$ configuration for the trigonal prism (i.e., $1^1A'_1 + 2^1A'_1 + 1^1E' + 2^1E' + ^3E' + ^3A'_2$), state-averaged calculations were performed for lowest 6 (singlet) or 3 (triplet) roots, followed by multi-state (MS) CASPT2[31]. Scalar relativistic effects were included at the second-order Douglas-Kroll level[32]. Spin-orbit coupling (SOC) was taken into account *a posteriori* using the state-interaction approach, i.e., by diagonalizing the SOC Hamiltonian in the basis set of perturbatively-modified states from MS-CASPT2, as implemented in the `Molcas` module RASSI[33]. Atomic mean-field integrals (AMFI) were used for the spin-orbit coupling calculations[34]. The same approach was used for simulation of magnetic properties, in particular the powder magnetic susceptibility and the effective magnetic moment at finite temperature using the method described in ref. 35.

For preliminary calculations (leading to the choice of the appropriate active space) and for simulations of SOC and magnetic properties, we used the following contraction of the ANO-RCC basis by Roos *et al.*[36]: 7s6p4d2f1g for Mo, 3s2p1d for C and N (the ANO-I basis). However, to obtain more accurate relative energetics reported in Table 1 we used a much larger contraction of the same basis: 10s9p9d6f4g2h for Mo, 5s4p3d2f1g for C and N (the ANO-II basis)[37]. The IPEA-shifted zero-order Hamiltonian was used in CASPT2 for the three values of the IPEA shift parameter: $\varepsilon_{\mathrm{IPEA}} = 0.25$ (the default), 0.5, and 0.75 a.u. The core electrons (i.e., below the Mo 4s level) were frozen during the CASPT2 calculations.

2.4 Coupled cluster calculations

Coupled cluster calculations were carried out either with `Molpro`[38] [RCCSD(T), UCCSD(T)] or `GAMESS` rev. May 2012 [CR-CC(2,3)][39], based of RHF/ROHF reference function, on top of the DFT:BP86-optimized geometries. The following basis sets were used: (A) cc-pwCVTZ-DK for Mo / cc-pVTZ-DK for C, N; (B) cc-pwCVTZ-DK for Mo / cc-pVDZ-DK for C,N; and (C) cc-pwCVnZ-PP for Mo / cc-pVnZ for C,N[40]. The results from (C) for $n =$T,Q were used to extrapolate the correlation energy to the infinite basis set according to the 'n^{-3}' formula by Helgaker *et al.*[41]. However, the relative singlet–triplet energy after the extrapolation differs by only 0.5 kcal/mol from the one obtained with basis (A) or (B). The core electrons (i.e., below the Mo 4s level) were frozen in all the coupled cluster calculations. Scalar relativistic effects were included either at the second-order Douglas-Kroll level[32] [basis sets (A), (B)] or via the relativistic pseudopotential for Mo [basis sets (C)].

2.5 Magnetic susceptibility measurements

Salt **1** has been synthesized as described in the literature (ref. 6). Magnetic susceptibility measurements were carried out on the MPMS XL SQUID magnetome-

ter (Quantum Design, Inc.) in the 3–300 K temperature range and external field of 2 kOe. Additional tests with a variable field (up to 10 kOe) were performed at $T = 100$ K and 200 K to confirm the linearity of $M(H)$. The sample of **1** ($m = 26.07$ mg), consisting of many single crystals, has been mounted to a plastic straw. Temperature- and field-dependent contribution of this addenda, measured separately, was accounted for to yield the magnetization of the sample.

A hyperbolic increase of χ was observed at $T < 50$ K and attributed in part to the addenda, in part to a trace contamination of the sample with a ubiquitous iron. We notice, however, that results in these low-T regime are not important for the presented interpretation. To remove the mentioned effect, as well as the constant diamagnetism, a function of form: $\chi_0 + C/T$ was fitted to the experimental data for $T < 150K$, yielding: $\chi_0 = -201.4 \cdot 10^{-6}$ emu/mol, $C = 25.42 \cdot 10^{-6}$ emu·K/mol. This function ($\chi_0 + C/T$) was then subtracted from the measured susceptibility to yield the results shown in Figure 5. The uncorrected susceptibility data are shown in Figure S9, ESI†.

3   Results and discussion

3.1   Preliminary considerations

The authors of ref. 6 suspected that it might be spin-orbit coupling (SOC) that lifts the degeneracy of the t_{2g} orbitals and thus leads to electron pairing. Such an effect is known in the literature; for instance, atomic lead is electronically diamagnetic in the spin-orbit coupled ground state ($^3P_0$, with $J = 0$)[42,43]. However, we shall demonstrate below by direct calculations (Section 3.4) that although the SOC clearly affects the effective magnetic moment of $[\mathrm{Mo(CN)}_6]^{2-}$, it cannot be responsible for the lack of paramagnetism.

Another hypothesis is that even if individual $[Mo(CN)_6]^{2-}$ anions may have, possibly, the triplet ground state, there could be an antiferromagnetic coupling in the solid state which leads to pairing of their magnetic momenta. However, if **1** were such an antiferromagnetic material, its Néel temperature would have to be much higher than the room temperature, meaning that the pairwise antiferromagnetic interaction should amount to at least a few kcal/mol (note that $R \cdot 300$ K $= 0.6$ kcal/mol). This is very unlike based on the large distance (8.9 Å) between the Mo centers and the lack of covalent bridges in the crystal structure of **1** (where there is only a water molecule in between the neighboring octahedra, interacting with the cyanide groups[6]). The overlap between magnetic orbitals of the neighboring Mo centers is expected to be very weak, too weak to explain the diamagnetic character.

Nevertheless, we performed DFT calculations for a simple model, namely the $[Mo(CN)_6]^{2-} \cdots H_2O \cdots [Mo(CN)_6]^{2-}$ motif, composed of two nearest-neighbor Mo centers and the water molecule in between, whose atomic coordinates were taken from the crystal structure of **1** (see Section 2.1 and ESI† for details). We evaluated the energy difference between the parallel ($\uparrow\uparrow$) and antiparallel ($\uparrow\downarrow$) alignment of the triplet spins on the neighboring Mo centers. This energy difference is on the order of only 0.1 kcal/mol (Table S1, ESI†) Moreover, lower energy is found for the parallel spin alignment than for the antiparallel one. Thus, not only the magnetic coupling is weak, consistently with the large distance between the two Mo centers and thus negligible overlap between their magnetic orbitals, but also the interaction slightly favors the parallel spin alignment. Therefore, the above "antiferromagnetic hypothesis" can be ruled out already at this preliminary stage, and the crystal structure of **1** can be considered as composed of magnetically dilute $[Mo(CN)_6]^{2-}$ centers.[44] In other words, the macroscopic diamagnetism observed for samples of **1** must be rooted in diamagnetic properties of $[Mo(CN)_6]^{2-}$ at the molecular level.

3.2 Structural properties

We thus studied the geometric and the electronic structure of $[\text{Mo(CN)}_6]^{2-}$ with quantum chemistry methods. Unsurprisingly, for the octahedral geometry the anion was found to have a triplet ground state, more than 10 kcal/mol below the lowest singlet state (see Section 3.3); this result fully conforms to qualitative predictions of the crystal field theory. However, we were surprised to see that $[\text{Mo(CN)}_6]^{2-}$ is actually not stable in the octahedral geometry. The harmonic frequency analysis at the DFT level reveals that the octahedral geometry (even if slightly distorted to D_{4h}, to account for unequal occupation of the t_{2g} level) is not an energy minimum, but a saddle point with two (triplet, singlet unrestricted) or four (singlet restricted) imaginary frequencies (see Table S2, ESI†), corresponding to deformation of the Mo–CN groups out of their octahedral arrangement. When the structure is slightly and allowed to relax in an unconstrained geometry optimization, it spontaneously adopts a *trigonal prismatic geometry*, which is an energy minimum. Both geometries, octahedron (unstable) and trigonal prism (stable) are shown in Figure 1.

The spontaneous conversion of the octahedron towards the trigonal prism was observed for both the hybrid (B3LYP) and nonhybrid (BP86) functional, and also when spin-orbit coupling was approximately accounted for within the ZORA approach (zero-order regular approximation). The conversion gives rise to a considerable energy gain, 7.3–13.5 kcal/mol (depending on the DFT method used) when calculated for the triplet state and even larger for the singlet state (see Table S4, ESI†). A comparable energy difference between the prism and the octahedron is also found with wave function methods, CCSD(T) and CASPT2 (Table S4, ESI†).

To further study the distortion process, we obtained the energy profile along the trigonal twist angle coordinate θ (Bailar twist), leading from octahedral ($\theta = 60°$) to trigonal form ($\theta = 0°$). The results are shown in Figure 2 and fully confirm that no activation energy is needed to covert the octahedral structure into the trigonal
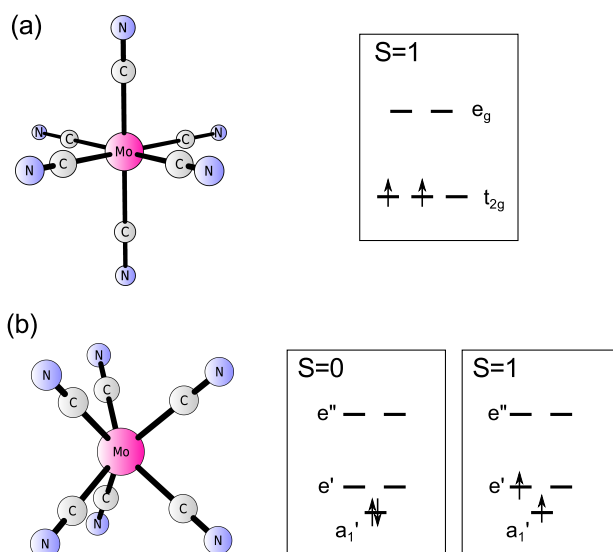
Figure 1 Octahedral (a) and trigonal prismatic (b) geometry of $[\text{Mo(CN)}_6]^{2-}$. The right panel shows schematically a splitting of the Mo d orbitals for both geometries and orbital occupancies in the triplet ground state for (a) and in close-lying singlet and triplet states for (b). For detailed structural parameters see Table S2, ESI†.
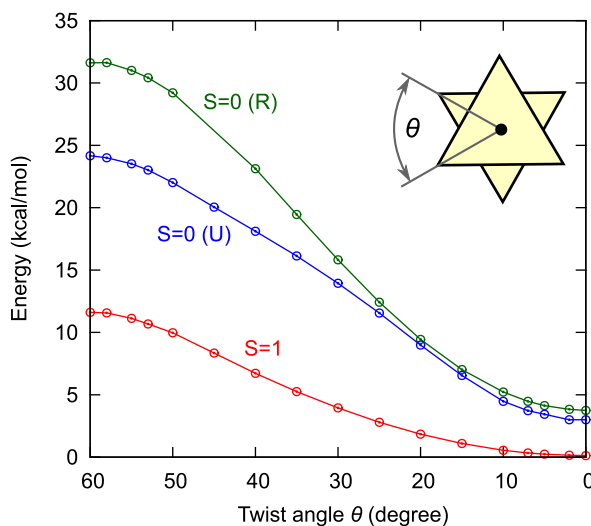

Figure 2 Scan of potential energy surface at the DFT:BP86/def2-TZVP level along the trigonal twist angle (Bailar twist coordinate), whose definition is shown graphically ($\theta = 60°$ for octahedron, $\theta = 0°$ for trigonal prism), for triplet ($S = 1$) and singlet state ($S = 0$) of isolated $[\text{Mo(CN)}_6]^{2-}$. The singlet state is either from spin-restricted (R) or spin-unrestricted (U) calculations; in the latter case the energy is corrected for spin contamination.

one. We also generated intrinsic reaction coordinate (IRC) paths starting from the (unstable) octahedral geometry, and leading ultimately to the (stable) trigonal prism structure (Figures S3–5 and video animations, ESI†). Interestingly, the computed IRC paths reveal a more complicated conversion mechanism than the simple Bailar twist scenario. After the system relaxes from the octahedral geometry (initial saddle point) it approaches another saddle point with no intervening minimum. Thus, from the endpoint of the first (IRC-1) path, we compute the subsequent (IRC-2) path, as shown in the ESI†. (In the case of triplet and unrestricted singlet there are even two such saddle points, in sequence, before reaching the final prismatic geometry and thus three consecutive IRC paths were needed.) The topology of potential energy surface emerging from our IRC studies is thus rather complicated and indicative of a bifurcation behavior[26]. In all cases the system eventually ends up in the trigonal prism form, while the energy along the reaction path goes monotonically downhill (ESI†).

We also notice that near the end of the IRC scan (after completing the IRC-2 path), the potential energy surface becomes very flat, suggesting that the system may easily ($\Delta E^{\ddagger} < 2$ kcal/mol) interconvert from one trigonal prismatic conformation to another via an intermediate structure which is similar to the end point of IRC-2 (see ESI†). In contrast, going back to the octahedral structure is an unlike event ($\Delta E^{\ddagger} > 10$ kcal/mol). The instability of the octahedron in favor of the trigonal prism and a noticeable lability of the latter structure (particularly for the triplet state) are also confirmed by Born-Oppenheimer molecular dynamics (MD) simulations. According to MD simulations (trajectories available as movies in the ESI†), the distortion of $[\text{Mo(CN)}_6]^{2-}$ out of the octahedral geometry is an extremely fast process, occurring on the sub-picosecond time scale. In sum, all our calculations for isolated $[\text{Mo(CN)}_6]^{2-}$ demonstrate that the distortion from the octahedron to the

trigonal prism geometry is thermodynamically favorable and barrierless, and hence the complex should not be isolated in the ideal octahedral geometry.

Trigonal prismatic ML_6 complexes are rare. However, it is well known that some ML_6 complexes—typically with $(d)^0$, $(d)^1$, or $(d)^2$ metal ions and σ-only ligands— do indeed adopt a trigonal prismatic geometry in order to maximize σ-donation from the ligands to the electron-deficient metal center[45,46]. The conversion from an octahedral to a trigonal prismatic structure can be viewed as the second-order Jahn-Teller (JT) distortion driven by mixing between two components of the t_{2g} level (empty or incompletely filled metal d orbitals) and two components of the highest occupied t_{1u} level (doubly-filled ligand orbitals), which appear in the same orbital symmetry (e') for the trigonal prismatic structure[47]. This mechanism is to be clearly distinguished from the first-order JT effect due to uneven occupation of the t_{2g} level. The latter effect is not expected to generate a significant distortion out of the octahedral geometry since the t_{2g} orbitals are not directed towards the ligands and mostly nonbonding[48].

We believe that $[Mo(CN)_6]^{2-}$ prefers the trigonal prismatic structure owing to the analogous reasons as for the other known prismatic ML_6 complexes, i.e., in order to maximize the metal–ligand σ-bonding interactions. Although cyanide can be both a σ-donor and a π-acceptor ligand, the molybdenum center in the high (+IV) oxidation state cannot efficiently donate to the empty π^* orbitals on the cyanide. Hence, with respect to the Mo(IV) center the cyanide behaves like a σ-only ligand (i.e., the π-backdonation plays a minor role). We notice that in a closely related $[Mo^{III}(CN)_6]^{3-}$ anion, where the Mo(III) center is a stronger π-donor towards the cyanide than the Mo(IV) one, both σ-donor and π-acceptor properties of the cyanide play a role in determining the geometry. Consequently, $[Mo^{III}(CN)_6]^{3-}$ is octahedral according both to the literature[49,50] and to the DFT calculations performed in this work (see Figure 3). Moreover, for a hypothetical $[Mo^{IV}Cl_6]^{2-}$ anion (i.e., cyanides
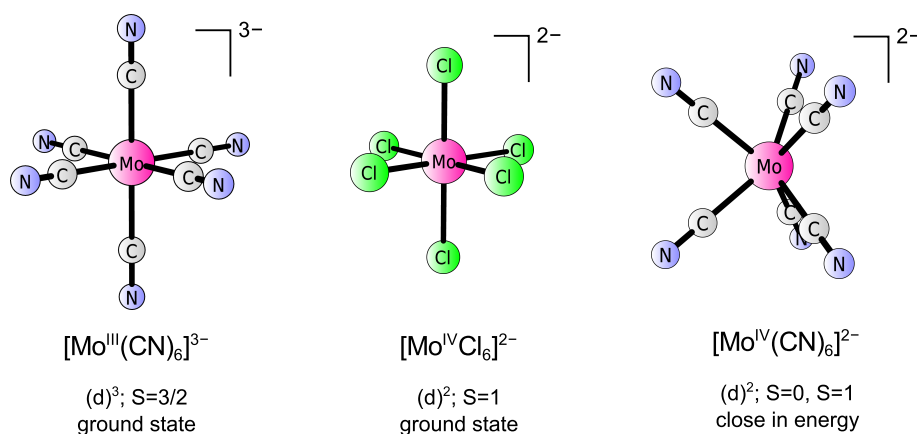
Figure 3 Comparison of the calculated structures and most stable spin-states for complex anions: $[\mathrm{Mo^{III}(CN)_6}]^{3-}$ (octahedral), $[\mathrm{Mo^{IV}Cl_6}]^{2-}$ (octahedral), and $[\mathrm{Mo^{IV}(CN)_6}]^{2-}$ (trigonal prismatic). Non-octahedral geometry in the case of $[\mathrm{Mo^{IV}(CN)_6}]^{2-}$ is due to a unique combination of strong σ-donation properties of the cyanide ligands and low number of d electrons on the Mo center, which suppresses π-backdonation to CN π^* orbitals.

replaced by chlorides) our DFT calculations also point to the octahedral geometry (Figure 3). This can be rationalized by a strong π-donor ability of the Cl ligands as compared with the CN ligands. Therefore, the trigonal prismatic structure in the case of $[\mathrm{Mo^{IV}(CN)_6}]^{2-}$ should be attributed to a unique combination of the σ-donor properties of cyanide with the high electrophilicity of Mo(IV) center.

In view of the above arguments, it is rather striking that the trigonal prismatic geometry of $[\mathrm{Mo(CN)_6}]^{2-}$ did not appear in the published crystal structure of **1**, which instead revealed the ideal octahedral geometry [6]. However, the calculations and discussions presented so far, apply to isolated $[\mathrm{Mo(CN)_6}]^{2-}$ anion in gas phase, whereas the situation in the crystal phase may be different. It is possible, at least in principle, that a steric crowding, hydrogen bonding, and other intermolecular interactions appearing in the solid state could stabilize the octahedral geometry of $[\mathrm{Mo(CN)_6}]^{2-}$, even though it is not an energy minimum for isolated gaseous anion.

To verify whether this might be the case, we performed periodic DFT geometry optimization, starting from the crystal structure of **1** from ref. 6 (exhibiting the ideal $[\mathrm{Mo(CN)_6}]^{2-}$ octahedra). The counterions $((\mathrm{CH_3})_4\mathrm{N^+})$ and water molecules were
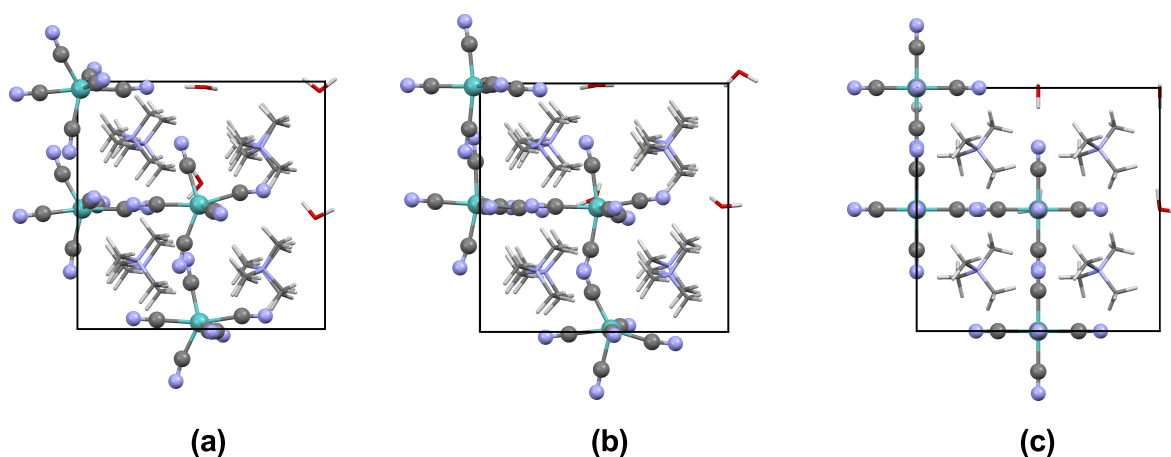
(a)   **(b)**   **(c)**

Figure 4 A view of the unit cell of **1** with the $\{[(CH_3)_4N][Mo(CN)_6]\cdot H_2O\}_4$ motif after the geometry has been optimized (in a frozen cell) in periodic DFT calculations assuming either the singlet (a) or the triplet (b) state for each Mo center; and the initial geometry (c), which was based on the published crystal structure of **1**. In the case (a) and (b) the $[Mo(CN)_6]^{2-}$ ions are notably distorted, adopting a geometry which is intermediate between the octahedron and the trigonal prism. Atomic coordinates in the ESI†.

obviously included in this simulation, as they are present in the published crystal structure. The calculations took into account various intermolecular interactions playing a role in the crystalline phase, including dispersion interactions (by means of the DFT-D2 approach of Grimme[28]). We thus believe that these periodic DFT calculations provide an adequate model of the situation in the solid state.

Nonetheless, even in these solid-state calculations, the $[Mo(CN)_6]^{2-}$ octahedra turned out to be unstable with respect to the similar distortion as observed for the isolated anion. During the simulation, the $[Mo(CN)_6]^{2-}$ anions adopted a highly distorted geometry, which is intermediate between the octahedron and the trigonal prism, and deviates considerably from the starting octahedral geometry (Figure 4). The strong deviation from the initial octahedral geometry was observed irrespective of which spin state (singlet or triplet) was assumed for individual $[Mo(CN)_6]^{2-}$ octahedra, although the distortion was larger for the singlet state. (This is consistent with a smaller energy gain from the trigonal twist and a greater structural lability in the case of triplet state, as found in Figure 2 and observed in the MD simulation.)

It thus follows that even the steric crowding and other intermolecular interactions in the crystalline state cannot fully overcome the preference of $[\text{Mo(CN)}_6]^{2-}$ to deviate from the octahedral geometry.

Clearly, we are aware that our periodic DFT simulation may not necessarily reach the global energy minimum, representing the correct structure of **1** in the solid state (it might have got stuck in a local energy minimum; however, it is not the goal of this study to predict the global minimum of the crystal structure, which is a complicated task even for small small organic molecules[51]). In spite of that, our periodic DFT simulation has clearly demonstrated that the published crystal structure of **1** is energetically unstable. It means that the ideal $[\text{Mo(CN)}_6]^{2-}$ octahedron does not correspond to a minimum on the potential energy surface, not even a local one. This holds true not only for single gaseous anion (where the correct geometry is undoubtedly the trigonal prism), but also for the model of crystalline phase. In the latter case, the correct geometry still remains uncertain, but the periodic DFT calculations point to highly distorted structure intermediate between the octahedron and the trigonal prism.

Therefore, the theory strongly suggests to take a critical look at the previously published crystal structure of **1**, because its high symmetry (leading to the octahedral geometry of $[\text{Mo(CN)}_6]^{2-}$) might be an artifact. For instance, the crystal structure may suffer from multiple twinning through merohedry (merohedral twinning)[52] or undiagnosed superstructure properties, or be disordered in such a way that standard crystallographic procedures give an incorrect "average structure" with too high a symmetry.[53–56] In consequence, the ideal octahedral arrangement of the CN ligands around the Mo center may be due to undiagnosed merohedral twinning, superstructure properties and/or disorder about some crystallographic symmetry element(s) (note that Mo is placed on a special position of very symmetric space group $Fm\bar{3}m$). It may be thus interesting to reinvestigate the previously published crys-

19

tal structure of **1**, with the aim of correcting a possible pitfall. However, modeling the suspected multiple twinning through merohedry and/or disorder for this highly-symmetric structure looks like a crystallographic endeavor. Certainly, this is beyond the the scope of the present study and would require a dedicated crystallographic paper.

In principle, a comparative IR/Raman analysis may be a powerful technique to discriminate between centrosymmetric and non-centrosymmetric structures. We thus compared the experimental IR and Raman data[6] with simulated wave numbers and intensities of the CN stretching vibrations (ν_{CN}), assuming different geometries and spin states of $[\text{Mo(CN)}_6]^{2-}$ (see Table S20, ESI†). However, the analysis turned out to be complicated due to accidental band overlapping and the fact that for $[\text{Mo(CN)}_6]^{2-}$ in the "octahedral geometry" the actual symmetry of the stationary point is not O_h, but D_{4h}, due to uneven occupation of the t_{2g} orbitals. The results are thus not fully conclusive, because the experimental distribution of the ν_{CN} bands is comparably similar to that calculated for either the trigonal prism in the singlet state (restricted) or the octahedron in the triplet state (cf Table S20). Hence, this comparative IR/Raman analysis neither confirms nor exclude the possibility of a trigonal prismatic geometry. One should also be aware that the experimental IR/Raman data reflects the situation in the solid state, where intermolecular interactions may shift the bands and affect their relative intensities as compared with the isolated anion.

Given that the true crystal structure of **1** is presently uncertain—in that we cannot resolve the discrepancy between the present theoretical calculations and the previously determined crystal structure—the rest of this paper is focused on the results for an isolated $[\text{Mo(CN)}_6]^{2-}$ anion as well as on their possible magnetic implications.

3.3   Spin-state energetics

It is clear that the mentioned distortion (from octahedral to trigonal prismatic structure) must seriously affect the relative spin-state energetics of $[\text{Mo(CN)}_6]^{2-}$. This could be already seen in previous Figure 2 above and is confirmed by the results of many methods gathered in Table 1. Whereas for the octahedral structure the triplet state is favored by at least 12 kcal/mol, for the prismatic structure the two spin states are lying closer in energy. All the DFT methods tested here still point to the triplet ground state, but now with the singlet state lying only a few kcal/mol above (which contrasts the situation for the octahedral geometry). However, it is well known that approximate DFT methods—while clearly useful for predicting molecular structures and providing a qualitatively correct landscape on the potential energy surface— might have problems with accurate description of spin-state energetics, for which an error of a few kcal/mol is not unlike[1,2,57]. In such problematic cases comparison with high-level wave function methods may be helpful to resolve the doubts. Therefore, to obtain more reliable energetics, we applied a multiconfigurational method, CASPT2 (perturbation theory based on the complete active space method;[58] for a review of applications to inorganic and bioinorganic systems see, e.g., ref. 59–61).

Before proceeding to the results, it must be recalled that CASPT2 is a perturbational method to include dynamical correlation on top of the variational CASSCF wave function[58]. The zero-order Hamiltonian in CASPT2 contains a parameter called the IPEA shift, whose default value ($\varepsilon_{\text{IPEA}} = 0.25$ a.u.) has been adjusted to correct a bias of the original formulation in favor of open-shell electronic structures[62]. Recently, a few authors attempted to vary the IPEA value and observed that the relative energetics of transition metal complexes can be very sensitive to the actual value of $\varepsilon_{\text{IPEA}}$ (at least for the standard choice of the active space in the preceding CASSCF calculations)[63,64]. The IPEA shift values as large as 0.5–1.0 a.u. have been found necessary to reproduce reference energetics, either based on experi-

Table 1 Relative spin-state energetics of $[\text{Mo(CN)}_6]^{2-}$ for the octahedral (oct) and trigonal prismatic (tp) structure ^{a}

	$E(\text{singlet}) - E(\text{triplet})$	
	oct	tp
DFT methods		
B3LYP	14.0	5.6
B3LYP*	13.1	4.3
OLYP	14.6	2.9
BP86	12.4	2.9
PBE	12.2	2.5
TPSS	12.6	5.4
TPSSh	14.0	7.2
M06	15.4	3.1
M06L	13.4	7.2
B2PLYP	14.7	4.3
Wave function methods		
CASPT2^{b,c}		
$(\varepsilon_{\text{IPEA}} = 0.25)$	12.9	2.7
$(\varepsilon_{\text{IPEA}} = 0.50)$	12.8	-1.3
$(\varepsilon_{\text{IPEA}} = 0.75)$	12.9	-4.6
RCCSD(T)	^{d}	5.6^e
		5.5^f
		5.1^g
UCCSD(T)^f	^{d}	6.4
CR-CC(2,3)^f	^{d}	6.6

^{a}In kcal/mol; positive number indicates triplet ground state. ^{b}CASPT2 energies calculated for the DFT-optimized structures (tp) or for the experimental structure (oct). ^{c}Basis set ANO-II (see Section 2.3) ^{d}Not determined. ^{e}Basis set (A). ^{f}Basis set (B). ^{g}Correlation energy extrapolated to infinite basis set using basis set (C) with $n =$T,Q. For basis sets (A)–(C) used in coupled cluster calculations see Section 2.4.

mental spin-state data[63] or high-level coupled cluster calculations[64], for the studied octahedral complexes of Fe and Co. In contrast, the default choice of $\varepsilon_{\text{IPEA}} = 0.25$ a.u. has been shown to overstabilize the high-spin state in the studied complexes[64]. Prompted by these literature results, we decided to test in this work the following three values of the IPEA shift parameter: 0.25, 0.50, and 0.75 a.u.

As can be seen from Table 1, the relative CASPT2 energy, indeed, strongly depends on the IPEA shift parameter. However, the dependence is observed only for the trigonal prismatic structure, not nearly for the octahedral one. Interestingly, for the prismatic structure, the ground state changes with increasing the $\varepsilon_{\text{IPEA}}$ parameter. Whereas for the IPEA shift of 0.25 a.u. the singlet–triplet splitting is similar as in the DFT calculations (i.e., the triplet ground state), for larger IPEA values (0.5 and 0.75 a.u.) the singlet clearly becomes the ground state favored by 1.5–5 kcal/mol. These numbers are adiabatic energies (i.e., each spin state computed in its equilibrium geometry). In the equilibrium geometry of the singlet state, the triplet is higher in energy already for the IPEA value of 0.25 a.u. (cf Table S8, ESI†). In sum, the CASPT2 calculations with a reasonable selection of the IPEA shift parameter indicate that $[\text{Mo(CN)}_6]^{2-}$ in the trigonal prismatic geometry may possibly have a singlet ground state.

For additional confirmation we also performed coupled cluster calculations: using the standard CCSD(T) method as well as completely renormalized CR-CC(2,3) method of Piecuch *et al.*[65] However, unlike CASPT2, both coupled cluster methods place the singlet state more than 5 kcal/mol above the triplet state. Therefore, the true spin-state energetics $[\text{Mo(CN)}_6]^{2-}$ still remains uncertain, but we notice that only the CASPT2 calculations (for $\varepsilon_{\text{IPEA}}$ larger than ~ 0.5 a.u.) are consistent with the experimental diamagnetic properties. In view of that, it is noteworthy that the lowest singlet state has a remarkable multiconfigurational character—caused by mixing of the principal configuration $[(a_1')^2(e')^0]$ with two excited configurations

23

$[(a_1')^0(e')^2]$ of the appropriate symmetry (see Table S5, ESI†). This multiconfigurational mixing, while correctly treated in the CASPT2 calculations, may be poorly described by single-reference coupled cluster methods. Moreover, it can be only partially taken into account in the spin-unrestricted DFT calculations (where a broken-spin solution was obtained, with fractionally-occupied natural orbital being basically the a_1' and one of the e' orbitals; see Figure S6 and Table S6, ESI†).

We notice that although the singlet and triplet states are predicted so close in energy, $[\text{Mo(CN)}_6]^{2-}$ is not expected to be a spin-crossover complex in the experimentally probed range of temperatures. This is because the free energy correction to the relative spin-state splitting is as small as ~ 0.5–1 kcal/mol at room temperature (Table S7, ESI†). Hence, if the electronic energy gap between the singlet and triplet spin states really amounts to ~ 5 kcal/mol (as suggested by CASPT2 with $\varepsilon_{\text{IPEA}} = 0.75$ a.u.), it will not be compensated by the thermal effects unless the temperature is very high. On the other hand, the low-lying excited triplet state, should influence the magnetic properties of **1** due to its non-zero Boltzmann population at elevated temperatures; we shall return to this observation later on.

3.4 Spin-orbit coupling

The energetics discussed so far did not include the effects of spin-orbit coupling (SOC). The SOC was taken into account at the CASSCF/CASPT2 level using a multi-state RASSI formalism (see Section 2.3 for details) by diagonalizing the appropriate relativistic Hamiltonian matrix in the basis set of all singlet and triplet states arising from the $(t_{2g})^2$ configuration for the octahedron or the corresponding $(a_1', e')^2$ configuration for the trigonal prism. The detailed results are provided in the ESI† (Tables S8–10). Although spin states with different multiplicities were allowed to interact via the SOC Hamiltonian, the mixing between singlet and triplet states

turned out to be very small, so that the resulting spin-orbit states largely retained their singlet or triplet character.

As might be expected, the SOC mainly affects spatially degenerate triplet states, by splitting them into multiplets, whereas the effect on the non-degenerate triplet states and the singlet states turned out to be negligible (~ 0.1 kcal/mol). For the experimental octahedral structure the lowest triplet term ($^3T_{1g}$) splits into three levels, yielding a ~ 3 kcal/mol wide multiplet (Table S8, ESI†). A comparable SOC effect is observed for the trigonal prismatic structure optimized for the singlet state (the ideal prism, D_{3h}), where the lowest triplet term ($^3E'$) is split to give a 2 kcal/mol wide multiplet (Table S9, ESI†). However, the triplet state is no longer orbitally-degenerate in its optimized geometry (distorted prism, C_{2v}); therefore, for this structure the triplet states undergoes only a negligible splitting due to the SOC by 0.1 kcal/mol (Table S10, ESI†).

It thus follows that the SOC interaction cannot drastically change the spin-state energetics of $[\mathrm{Mo(CN)_6}]^{2-}$, its main effect being an additional stabilization of the lowest term emerging from the triplet state by ~ 1 kcal/mol for the more symmetric structures (O_h, D_{3h}). In variance, the effect nearly disappears for the less symmetric structure (C_{2v}) being the optimal geometry of the triplet state.

3.5 Magnetic properties

The above multi-state RASSI formalism with the SOC interaction was also used to simulate the magnetic properties of $[\mathrm{Mo(CN)_6}]^{2-}$. It is worthy to look at the effective magnetic moment (μ_{eff}), whose temperature dependence reflects contributions of all thermally available energy levels[35]. Table 2 shows the temperature dependence of μ_{eff} for the three representative geometries of $[\mathrm{Mo(CN)_6}]^{2-}$ considered above: the octahedron and the optimized (trigonal prismatic) structures of the singlet state

Table 2 Effective magnetic moment of $[\mathrm{Mo(CN)_6}]^{2-}$ (Bohr magneton) for experimental octahedral (oct) and calculated trigonal prismatic structure, optimized either for singlet (^{1}tp) or triplet state (^{3}tp).[a]

T (K)	oct	^{1}tp (D_{3h})	^{3}tp (C_{2v})
5	1.10	$5 \cdot 10^{-3}$	2.46
10	1.21	$7 \cdot 10^{-3}$	2.65
50	1.37	0.017	2.77
100	1.52	0.094	2.78
200	1.77	0.56	2.78
300	1.99	1.04	2.79
Spin-only value for $S = 1$: $\mu_0 \approx 2.83$			

[a]RASSI calculations based on perturbatively modified states from MS-CASPT2, $\varepsilon_{\mathrm{IPEA}} = 0.25$ a.u., basis ANO-I.

(^{1}tp) and the triplet state (^{3}tp). Results for these geometries will be now discussed in a different order for the sake of clarity.

The magnetic moment calculated for the ^{3}tp structure (the distorted prism, C_{2v}) is nearly constant and close to the spin-only value. In contrast, for the octahedral structure the magnetic moment is considerably below the spin-only value, particularly at low temperatures. This is due to a partial quenching of the spin momentum by the angular momentum in the degenerate triplet state ($^3T_{1g}$). Nevertheless, the paramagnetic character is still remarkable in the whole range of temperatures. Finally, for the ^{1}tp structure (the ideal trigonal prism, D_{3h}), the magnetic moment is nearly zero at low temperatures because for this structure the lowest energy state is diamagnetic singlet. (Note that, in contrast to adiabatic CASPT2 energies presented in Table 1, for the optimized ^{1}tp geometry, the singlet is vertically below the triplet already for $\varepsilon_{\mathrm{IPEA}} = 0.25$ a.u.; cf Table S8 in the ESI†.) Interestingly, with increasing temperature, μ_{eff} increases to 40% of the spin-only value at room temperature. As mentioned above, this is a consequence of growing a Boltzmann population of the excited triplet state.

Clearly, the numeric μ_{eff} results for the ^{1}tp structure in Table 2 are not to be taken quantitatively since they critically depend on the singlet–triplet splitting, whose ac-

tual value is presently uncertain (see Section 3.3). However, if $[Mo(CN)_6]^{2-}$ has indeed a singlet ground state and a triplet state only a few kcal/mol above, these data suggest that the magnetic susceptibility should reflect—in addition to the dominant diamagnetism due to the singlet state—also the Boltzmann population of the paramagnetic triplet state. The appropriate model for such a two-level system (singlet ground state, triplet excited state) is developed in the ESI†. The magnetic susceptibility χ_{para} in this model (not accounting for constant diamagnetic contribution) can be expressed by the following function of the temperature (T):

$$f(T) = \frac{a/T}{1 + \frac{1}{3}\exp(\Delta/kT)}, \tag{1}$$

Δ being the singlet–triplet splitting. The dimensionless constant a equals to unity if the triplet state has a spin-only magnetic moment ($2\sqrt{2}$ Bohr magneton); by setting a to a smaller value, one may effectively describe a quenching of the magnetic moment due to the SOC. We notice that eq. (1) is similar to the Bleaney–Bowers formula used to describe the magnetic susceptibility of an antiferromagnet[66].

A more realistic description of the SOC can be provided by considering that the triplet state splits into three Krammer's doublets (assuming the ideal prismatic geometry characteristic of the singlet state). To account for this effect, additional simulations of magnetic susceptibility were carried out with the RASSI approach (see above), in which the wave functions for the singlet and triplet state were taken from the CASSCF calculations, but their initial splitting (i.e., prior to adding the SOC interaction) was considered an adjustable parameter, analogous to the parameter Δ in the above analytic function [eq. (1)].

Figure 5 shows the experimental magnetic susceptibility of **1** compared with these two theoretical models. For clarity of presentation, the experimental data were corrected by subtracting a constant diamagnetic susceptibility ($\chi_0 = -201.4 \cdot 10^{-6}$ emu/mol) and a trace paramagnetism observed at low temperatures (C/T with
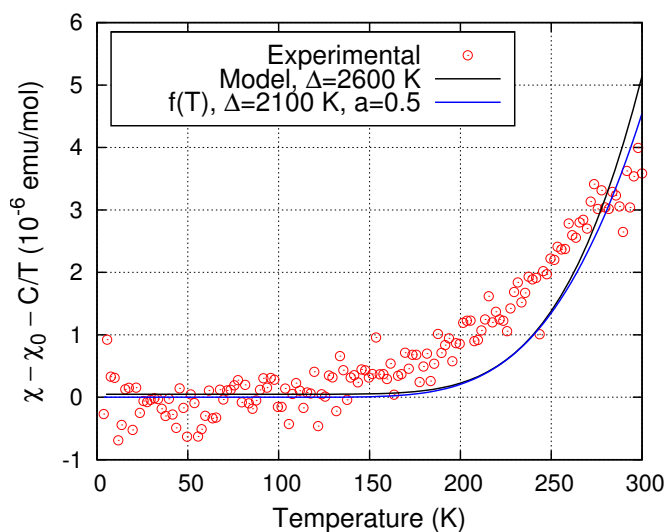
Figure 5 Molar magnetic susceptibility of **1** recorded on the SQUID magnetometer (after subtracting the χ_0 and C/T terms, where $\chi_0 = -201.4 \cdot 10^{-6}$ emu/mol, $C = 25.42 \cdot 10^{-6}$ emu·K/mol, as explained in Figure S9, ESI†) *versus* theoretical predictions from two models (see text) with the adjusted values of the Δ parameter. The increase of susceptibility for $T > 100$–150 K is tentatively attributed to increasing a Boltzmann population of the excited triplet state.

$C = 25.42 \cdot 10^{-6}$ emu·K/mol). The latter effect may be attributed to contamination of the sample with ubiquitous iron and is not of our interest in this study. (See Section 2.5 for more details and Figure S9 in the ESI† for uncorrected magnetic data.)

It is clear from experimental data in Figure 5 that **1** remains diamagnetic in the whole range of temperatures probed in the experiment. However, it also turns out that χ actually increases by ca. $+4 \cdot 10^{-6}$ emu/mol when T increases from ~ 100 to 300 K. This increase is small compared with the total diamagnetic susceptibility ($\chi_0 \sim -2 \cdot 10^{-4}$ emu/mol), but it would be very difficult to explain this effect otherwise than by invoking the Boltzmann population of the low-lying paramagnetic state. Moreover, as shown in Figure 5, both theoretical approaches (i.e., the analytic function (1) with $a = 1/2$ and the numerical model) can roughly reproduce such an increase of χ assuming reasonable values for the Δ parameter (2100–2600 K, i.e., 4–5 kcal/mol). These values are not far from the singlet–triplet gaps obtained

from the CASPT2 calculations with the increased IPEA shift (cf Table 1). Note, however, that both theoretical approaches give the $\chi(T)$ functions which are too convex to ideally fit the experimental data. Moreover, since the experimental effect is small and there still remains a controversy about the structure of $[\mathrm{Mo(CN)_6}]^{2-}$ (contradiction between computational and crystallographic structure; see Section 3.2), the interpretation presented in this section and especially in Figure 5 should be considered a hypothesis. By proposing it, we clearly do not claim that we have found a definite explanation of the experimental magnetic behavior of **1**. This must await correct re-determination of the crystal structure, which is beyond the scope of this work (see Section 3.2).

4   Conclusions

The calculations carried out in this work confirmed that, assuming the previously reported octahedral geometry of $[\mathrm{Mo(CN)_6}]^{2-}$, this anion would have a triplet ground state, favored over the lowest singlet state by more than 10 kcal/mol. Moreover, the presented calculations also indicated that neither spin-orbit coupling on a single site, nor magnetic interactions between neighboring sites in the previously published crystal structure of **1** (their Mo centers being separated by more than 8 Å distance), could give rise to the diamagnetic behavior in the broad range of temperatures. All these results make it impossible to understand the experimentally well confirmed diamagnetic properties of salt **1**, containing the $[\mathrm{Mo(CN)_6}]^{2-}$ anion, if the anion is indeed octahedral.

However, the calculations surprisingly revealed that an isolated $[\mathrm{Mo(CN)_6}]^{2-}$ anion is unstable in the octahedral geometry; it undergoes (very quickly and spontaneously) a distortion to give trigonal prismatic geometry. The distortion was found to be energetically favorable and barrierless, because the octahedral geometry

is not even a minimum, but a saddle point on the potential energy surface. The tendency of $[Mo(CN)_6]^{2-}$ to adopt the trigonal prism geometry was rationalized as a second-order Jahn-Teller effect, which is governed by the strong σ-donation from the cyanides to the electron deficient Mo(IV) center, compared with lacking or very weak π-donation and π-backdonation effects. The mechanism is thus analogous as for several known trigonal prismatic ML_6 complexes[45,46]. Nonetheless, while most of them contains hydride, alkyl or dithiolene ligands, $[Mo(CN)_6]^{2-}$ may be the first example of a non-octahedral complex based on cyanide ligands ("may be"—because this is so far only a computational result; not yet confirmed by the crystal structure).

According to the calculations, the distortion of the $[Mo(CN)_6]^{2-}$ geometry—from the octahedron to the trigonal prism—may give rise to a significant stabilization of the singlet with respect to the triplet state. This effect is rooted in a stronger σ-donation in the singlet than in the triplet state (thus, basically, the singlet gains more from the distortion than the triplet). Although the qualitative effect is very apparent, the actual energy difference between the two spin states still remains uncertain because various computational methods applied here (DFT, CASPT2, and coupled cluster) gave a considerable variation of the results. In passing we highlight the need of accurate and reliable computational protocols to unambiguously predict the spin-state energetics of transition metal complexes, including those with significant multireference character. Herein, only the CASPT2 calculations (with the IPEA shift parameter greater than 0.5 a.u.) were able to recover the singlet ground state, in agreement with the diamagnetic character of salt **1**. According to these calculations, the first triplet excited state is lying low enough in energy to be thermally populated at elevated temperatures and thus its presence should affect the magnetic susceptibility. This prediction seems to be consistent with a slight increase of the susceptibility with increasing the temperature that was revealed in the SQUID measurements of **1**. However, the remaining uncertainty about the crys-

tal structure (see below) prevent us from drawing very definite conclusions. In this regard, the proposed explanation of the magnetic properties of **1** should be treated as a hypothesis.

An important and intriguing output of this work is the lack of agreement between the computational and crystallographic structure of $[Mo(CN)_6]^{2-}$ anion. Whereas the crystal structure in ref. 6 depicted the anion in the ideal octahedral geometry (which has been paradoxical since the beginning, in view of the diamagnetism), this work has shown that the octahedral geometry not only would be inconsistent with the diamagnetism, but it also turned out to be unstable with respect to the mentioned second-order Jahn-Teller distortion, and thus should not be isolated. The instability of octahedron was observed here not only for single gaseous anion, but also for periodic DFT model of the crystalline state of **1**. Our periodic DFT optimization yielded a highly distorted structure that is very different from the previously reported crystal structure, although the latter was used as the starting point for our simulations. Such a result is surprising and unexpected when a correct crystal structure is used as the starting point.

The presented theoretical arguments against the octahedral structure are strong, as they are based on multiple approaches: harmonic frequency analysis, energy calculations with various methods, potential energy scan along the Bailar twist coordinate, IRC paths, MD simulations, and even periodic DFT to model the situation in the solid state. All these methods point to a similar conclusion that $[Mo(CN)_6]^{2-}$ should not be isolated in the octahedral geometry. Having learned all that from theory and knowing the experimentally well confirmed diamagnetic properties of **1**, we are thus left with no other choice than to suppose that there might be an error in the previous crystal structure determination. For instance, it is possible that due to a (multiple) merohedral twinning and/or disorder which were not accounted for correctly, or due to overlooked superstructure properties, the very high crystallo-

graphic symmetry ($Fm\bar{3}m$) might be an artifact, leading to wrong arrangement of the CN ligands around the Mo center; i.e., a kind of "average structure." Before this controversy is resolved in full (by revisiting and possibly correcting the crystal structure) it is not legitimate to give definite conclusions about the magnetism of **1**. However, the problems with this crystal structure look like very challenging from the crystallographic point of view. According to our experience, resolving them may require developing an appropriate structural model to describe the multiple merohedral twinning and/or disorder in the high-symmetry space group. While clearly beyond the scope of this work, it may be worthy to consider such possibilities in subsequent crystallographic studies of **1**, in order to depict the true molecular structure of $[\mathrm{Mo(CN)_6}]^{2-}$ anion, which—according to the present theoretical findings and its magnetic properties—is very unlikely to be octahedral.

Acknowledgments

References

[1] (a) Swart, M. *Int. J. Quantum Chem.* **2013**, *113*, 2–7; (b) Swart, M. *J. Chem. Theory Comput.* **2008**, *4*, 2057–2066.

[2] Ghosh, A. *JBIC J. Biol. Inorg. Chem.* **2006**, *11*, 712–724.

[3] Harvey, J. N. *Struct. Bonding* **2004**, *112*, 151–183.

[4] Radoń, M. *Phys. Chem. Chem. Phys.* **2014**, *16*, 14479–14488.

[5] Kutzelnigg, W. *Angew. Chem. Int. Ed.* **1996**, *35*, 572–586.

[6] Szklarzewicz, J.; Matoga, D.; Niezgoda, A.; Yoshioka, D.; Mikuriya, M. *Inorg. Chem.* **2007**, *46*, 9531–9533.

[7] Wang, X.-Y.; Avendaño, C.; Dunbar, K. R. *Chem. Soc. Rev.* **2011**, *40*, 3213–3238.

[8] Tokoro, H.; Ohkoshi, S.-i. *Dalton Trans.* **2011**, *40*, 6825–6833.

[9] TURBOMOLE version 5.9 and 6.5, a development of University of Karlsruhe and Forschungszentrum Karlsruhe GmbH, 1989–2007, TURBOMOLE GmbH, since 2007; available from http://www.turbomole.com.

[10] Frisch, M. J. *et al.* Gaussian 09 Revision C.01. Gaussian Inc. Wallingford CT 2009.

[11] Weigend, F.; Ahlrichs, R. *Phys. Chem. Chem. Phys.* **2005**, *7*, 3297–3305.

[12] (a) Weigend, F.; Furche, F.; Ahlrichs, R. *J. Chem. Phys.* **2003**, *119*, 12753–12762; (b) Weigend, F.; Häser, M.; Patzelt, H.; Ahlrichs, R. *Chem. Phys. Lett.* **1998**, *294*, 143–152.

[13] (a) Becke, A. D. *Phys. Rev. A* **1988**, *38*, 3098–3100; (b) Perdew, J. P. *Phys. Rev. B* **1986**, *33*, 8822–8824.

[14] Perdew, J. P.; Burke, K.; Ernzerhof, M. *Phys. Rev. Lett.* **1996**, *77*, 3865–3868.

33

[15] (a) Becke, A. D. *J. Chem. Phys.* **1993**, *98*, 5648–5652; (b) Stephens, P. J.; Devlin, F. J.; Chabalowski, C. F.; Frisch, M. J. *J. Phys. Chem.* **1994**, *98*, 11623–11627.

[16] Tao, J.; Perdew, J. P.; Staroverov, V. N.; Scuseria, G. E. *Phys. Rev. Lett.* **2003**, *91*, 146401–146404.

[17] Perdew, J. P.; Tao, J.; Staroverov, V. N.; Scuseria, G. E. *J. Chem. Phys.* **2004**, *120*, 6898–6911.

[18] Grimme, S. *J. Chem. Phys.* **2006**, *124*, 034108.

[19] Reiher, M.; Salomon, O.; Hess, B. A. *Theor. Chem. Acc.* **2001**, *107*, 48–55.

[20] Handy, N. C.; Cohen, A. J. *Mol. Phys.* **2001**, *99*, 403–412.

[21] (a) Zhao, Y.; Truhlar, D. G. *Theor. Chem. Acc.* **2008**, *120*, 215–241; (b) Zhao, Y.; Truhlar, D. G. *J. Chem. Phys.* **2006**, *125*, 194101.

[22] (a) Yamaguchi, K.; Takahara, Y.; Fueno, T.; Houk, K. *Theor. Chim. Acta* **1988**, *73*, 337–364; (b) Yamaguchi, K.; Jensen, F.; Dorigo, A.; Houk, K. *Chem. Phys. Lett.* **1988**, *149*, 537–542.

[23] Zheng, J.; Xu, X.; Truhlar, D. G. *Theor. Chem. Acc.* **2011**, *128*, 295–305.

[24] ADF2013, SCM, Theoretical Chemistry, Vrije Universiteit, Amsterdam, The Netherlands, http://www.scm.com.

[25] (a) van Lenthe, E.; Snijders, J. G.; Baerends, E. J. *J. Chem. Phys.* **1996**, *105*, 6505; (b) van Lenthe, E.; Ehlers, A.; Baerends, E.-J. *J. Chem. Phys.* **1999**, *110*, 8943.

[26] (a) Ess, D.; Wheeler, S. W.; Iafe, R.; Xu, L.; Çelebi-Ölçüm, N.; Houk, K. N. *Angew. Chem. Int. Ed.* **2008**, *47*, 7592–7601; (b) Maeda, S.; Harabuchi, Y.;

34

Ono, Y.; Taketsugu, T.; Morokuma, K. *Int. J. Quantum Chem.* **2015**, *115*, 258–269.

[27] Soler, J. M.; Artacho, E.; Gale, J. D.; García, A.; Junquera, J.; Ordejón, P.; Sánchez-Portal, D. *J. Phys.: Cond. Matt.* **2002**, *14*, 2745.

[28] Grimme, S. *J. Comp. Chem.* **2006**, *27*, 1787–1799.

[29] Troullier, N.; Martins, J. L. *Phys. Rev. B* **1991**, *43*, 1993–2006.

[30] Aquilante, F.; De Vico, L.; Ferré, N.; Ghigo, G.; Malmqvist, P.-Å.; Neogrády, P.; Pedersen, T. B.; Pitoňák, M.; Reiher, M.; Roos, B. O.; Serrano-Andrés, L.; Urban, M.; Veryazov, V.; Lindh, R. *J. Comp. Chem.* **2010**, *31*, 224–247.

[31] Finley, J.; Malmqvist, P.-Å.; Roos, B. O.; Serrano-Andres, L. *Chem. Phys. Lett.* **1998**, *288*, 299–306.

[32] Reiher, M.; Wolf, A. *J. Chem. Phys.* **2004**, *121*, 10945–10956.

[33] Malmqvist, P. Å.; Roos, B. O.; Schimmelpfennig, B. *Chem. Phys. Lett.* **2002**, *357*, 230–240.

[34] Hess, B. A.; Marian, C. M.; Wahlgren, U.; Gropen, O. *Chem. Phys. Lett.* **1996**, *251*, 365–371.

[35] Vancoillie, S.; Rulíšek, L.; Neese, F.; Pierloot, K. *J. Phys. Chem. A* **2009**, *113*, 6149–6157.

[36] Roos, B. O.; Lindh, R.; Malmqvist, P.-Å.; Veryazov, V.; Widmark, P.-O. *J. Phys. Chem. A* **2005**, *109*, 6575–6579.

[37] The bug in the `Molcas` basis library with the ANO-RCC basis set for C atom, which was revealed in January 2015 (see: `http://www.molcas.org/ANO`, accessed March 2015), has been corrected in the present calculations. However,

the difference between the final CASPT2 spin-state energetics in Table 1 computed with the corrected and original basis set is only 0.2–0.4 kcal/mol.

[38] Werner, H.-J. *et al.* MOLPRO, version 2012.1, a package of ab initio programs, see `http://www.molpro.net` (accessed Jul 2014).

[39] Schmidt, M. W.; Baldridge, K. K.; Boatz, J. A.; Elbert, S. T.; Gordon, M. S.; Jensen, J. H.; Koseki, S.; Matsunaga, N.; Nguyen, K. A.; Su, S.; Windus, T. L.; Dupuis, M.; Montgomery, J. A. *J. Comp. Chem.* **1993**, *14*, 1347–1363.

[40] Peterson, K. A.; Figgen, D.; Dolg, M.; Stoll, H. *J. Chem. Phys.* **2007**, *126*, 124101.

[41] Helgaker, T.; Klopper, W.; Koch, H.; Noga, J. *J. Chem. Phys.* **1997**, *106*, 9639–9646.

[42] Hawk, R. M.; Sharp, R. R. *J. Chem. Phys.* **1974**, *60*, 1009–1016.

[43] Armbruster, M. K.; Weigend, F.; van Wullen, C.; Klopper, W. *Phys. Chem. Chem. Phys.* **2008**, *10*, 1748–1756.

[44] Note that although in Section 3.2 we argue that the previous crystal structure might be incorrect in regard to the CN orientations around the Mo center, the positions of Mo atoms and thus the Mo$\cdots$Mo distance (~ 8.9Å) should be determined reliably. This is because Mo is much heavier ($Z = 42$) than other atoms present in this crystal structure. Also in our periodic DFT calculations, although the $[\text{Mo(CN)}_6]^{2-}$ structure deviates noticeably from the ideal octahedron and the Mo centers are no longer symmetry equivalent, the nearest neighbor Mo$\cdots$Mo distance never drops below 8 Å (it varies from 8.3 to 9.2 Å). Therefore, the basic argument given here—that due to the large and non-covalent Mo$\cdots$Mo distance, the magnetic coupling is far too weak to account

for the diamagnetic properties (on the order of 0.1 kcal/mol, instead of a few kcal/mol)—should hold true.

[45] Kaupp, M. *Chem. Eur. J.* **1998**, *4*, 1678–1686.

[46] (a) Pfennig, V.; Seppelt, K. *Science* **1996**, *271*, 626–628; (b) Seppelt, K. *Acc. Chem. Res.* **2003**, *36*, 147–153.

[47] (a) Kang, S. K.; Tang, H.; Albright, T. A. *J. Am. Chem. Soc.* **1993**, *115*, 1971–1981; (b) King, R. *J. Organometal. Chem.* **2001**, *623*, 95–100.

[48] Pearson, R. G. *Proc. Natl. Acad. Sci.* **1975**, *72*, 2104–2106.

[49] Beauvais, L. G.; Long, J. R. *J. Am. Chem. Soc.* **2002**, *124*, 2110–2111.

[50] Hendrickx, M. F. A.; Mironov, V. S.; Chibotaru, L. F.; Ceulemans, A. *J. Am. Chem. Soc.* **2003**, *125*, 3694–3695.

[51] Price, S. L. *Chem. Soc. Rev.* **2014**, *43*, 2098–2111.

[52] Massa, W. *Crystal Structure Determination*, 2nd ed.; Springer-Verlag: Berlin Heidelberg New York, 2004; Chapter 11.

[53] Examples of similar effects are known in the literature. For instance, $CsMnF_4$ (ref. 52 and 54) can be solved reasonably in the $P4/mmm$ space group (apparent too high symmetry) to give the wrong "average structure," lacking the expected Jahn-Teller elongation. The correct geometry only appears if the structure is solved as a merohedral twin in the $P4/n$ space group . Another example is the long-lasting debate on the structure of β-cristobalite (see for instance ref. 55 and references therein). The original structure (by Wyckoff) had the linear Si–O–Si angles, but this is chemically unacceptable and in contrast to bent Si–O–Si motifs found in other forms of silica. Only later it has been shown that the structure can be better refined using disordered models with the bent

Si–O–Si motifs and the O atoms occupying (either random or specified) positions on a circle around the Si⋯Si axis. Finally, in crystal structures of some metal–nitrosyl complexes the M–N–O unit appears as linear although the bend one is expected based on spectroscopy and/or quantum chemical calculations (ref. 56). This is explained by undiagnosed disorder, which may be difficult to eliminate if the complex molecule is placed on a special position, such as a crystallographic symmetry axis (cf ref. 56.b).

[54] Molinier, M.; Massa, W. *Z. Naturforsch.* **1992**, *47b*, 783–788.

[55] Liu, F.; Garofalini, S. H.; King-Smith, R.; Vanderbilt, D. *Phys. Rev. Lett.* **1993**, *70*, 2750–2753.

[56] (a) Pratt, C. S.; Coyle, B. A.; Ibers, J. A. *J. Chem. Soc. A* **1971**, 2146–2151; (b) Thyagarajan, S.; Incarvito, C. D.; Rheingold, A. L.; Theopold, K. H. *Inorg. Chim. Acta* **2003**, *345*, 333–339; (c) Tomson, N. C.; Crimmin, M. R.; Petrenko, T.; Rosebrugh, L. E.; Sproules, S.; Boyd, W. C.; Bergman, R. G.; DeBeer, S.; Toste, F. D.; Wieghardt, K. *J. Am. Chem. Soc.* **2011**, *133*, 18785–18801.

[57] Cramer, C. J.; Truhlar, D. G. *Phys. Chem. Chem. Phys.* **2009**, *11*, 10757–10816.

[58] Andersson, K.; Roos, B. O. *Int. J. Quantum Chem.* **1993**, *45*, 591–607.

[59] Pierloot, K. *Mol. Phys.* **2003**, *101*, 2083–2094.

[60] Pierloot, K. *Int. J. Quantum Chem.* **2011**, *111*, 3291–3301.

[61] Chen, H.; Lai, W.; Shaik, S. *J. Phys. Chem. B* **2011**, *115*, 1727–1742.

[62] Ghigo, G.; Roos, B.; Malmqvist, P.-Å. *Chem. Phys. Lett.* **2004**, *396*, 142–149.

[63] Kepenekian, M.; Robert, V.; Le Guennic, B. *J. Chem. Phys.* **2009**, *131*, 114702.

[64] Lawson Daku, L. M.; Aquilante, F.; Robinson, T. W.; Hauser, A. *J. Chem. Theory Comput.* **2012**, *8*, 4216–4231.

[65] (a) Piecuch, P.; Włoch, M.; Gour, J. R.; Kinal, A. *Chem. Phys. Lett.* **2006**, *418*, 467–474; (b) Shen, J.; Piecuch, P. *Chem. Phys.* **2012**, *401*, 180–202.

[66] Bleaney, B.; Bowers, K. D. *Proc. Roy. Soc. A* **1951**, *214*, 451–465.

Graphical and textual abstract for the TOC entry
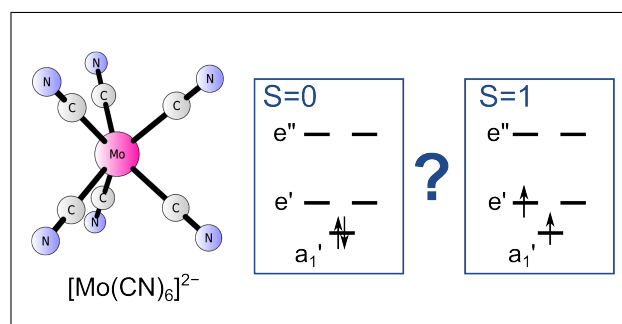
$[\mathrm{Mo(CN)_6}]^{2-}$ is computationally predicted to be a trigonal prismatic complex with closely-lying singlet ($S = 0$) and triplet ($S = 1$) spin states.